COBEM UBERLÂNDIA 2019

ABCM Associação Brasileira de Engenharia e Ciências Mecânicas

25th ABCM International Congress of Mechanical Engineering
October 20-25, 2019, Uberlândia, MG, Brazil

COB-2019-0592
VISUALIZATION OF VISCOPLASTIC FLUID FLOW IN AN ABRUPT CONTRACTION USING PARTICLE IMAGE VELOCIMETRY

Yamid J. García Blanco
Vitor Yoshiharu Urazaki
Eduardo Matos Germer
Admilson T. Franco
Federal University of Technology-Paraná - UTFPR, Research Center for Rheology and Non-Newtonian Fluids - CERNN, 81280-340, Rua Deputado Heitor Alencar Furtado 5000 - Ecoville, Curitiba-PR, Brazil
yjgarcia.blanco@gmail.com, vitor.urazaki@gmail.com, eduardomg@utfpr.edu.br, admilson@utfpr.edu.br.

Abstract. *Viscoplastic fluid flows through sudden contractions can be found in several industrial processes, such as polymer extrusion, food pumping, and drilling of oil wells. However, there are not enough experimental studies focused on the visualization of this kind of flow. This paper presents an experimental study of viscoplastic fluid flow in a cylindrical axisymmetric contraction facility (1.85 contraction ratio). Aqueous solutions with different weight percent of Carbopol are used as a viscoplastic fluid, characterized by the Herschel-Bulkley model. Particle Image Velocimetry (PIV) is used as a visualization technique to obtain detailed measurements of mean velocity, velocity fluctuations (axial and radial), and vortex structures generation. A stage for validation of the methodology used with the PIV technique was performed for water in a straight tube at turbulent flow conditions, and the data were compared with numerical and other experimental studies in the literature. For viscoplastic flow through the contraction was studied the mean axial velocity, the dependence of the appearance of vortex structure and unyielded zones in the contraction corners and the plug region, and the variation of the pressure losses with the increasing of Reynolds number. As the Reynolds number is approaching the turbulent regime, larger shear rates are generated at the contraction, reducing the area of the unyielded regions and promoting the appearance of large vortex structures at the corners of the abrupt contraction.*

Keywords: *Viscoplastic fluid, Herschel-Bulkley, experimental study, contraction, unyielded, PIV.*

1. INTRODUCTION

The present study deals with the flow of viscoplastic fluids through abrupt contractions, that are commonly encountered in industrial processes such as polymer mold filling, oil well drilling, among others.

In the oil industry, non-Newtonian materials such as slurries, xanthan gum, sucrose, and polymer solutions are commonly used, some of them as drilling fluids (Kfuri *et al.*, 2011). The drilling fluid used during the drilling of oil wells flows into a drill string and inner channels, which implies the passage through sudden contractions. This results in pressure and energy losses (Fester *et al.*, 2008), the appearance of secondary flow regions such as vortex structures at the upstream zone (1)(Jay *et al.*, 2002), as detailed at Fig. 1.

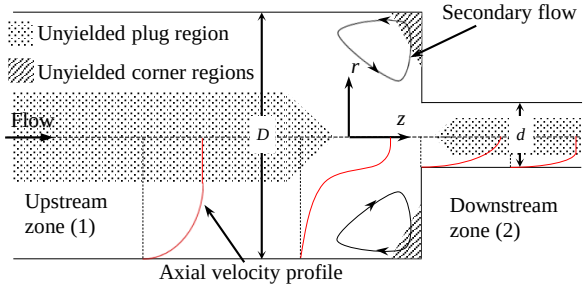

Figure 1. Schematic diagram of a viscoplastic fluid flow through an abrupt circular contraction

The flow of viscoplastic fluids in tubes with sudden area reduction has a particular structure, where the laminar fully developed flow in the entrance and exit tubes consist of peripheral viscous flow zones and an unyielded plug zone around the central axis of the duct. In the contraction corners, it is possible to have vortex structures or unyielded regions and in

some cases, the coexistence of both conditions (Jay *et al.*, 2002). As the flow approaches the contraction, high shear rate and pressure drops appear and flow velocity increases as the fluid enters to the downstream zone (2) (Kim-e *et al.*, 1983), as shown in Fig. 1. The size of the unyielded regions depends on the flow behavior index (n) and the Herschel-Bulkley number (HB), also known as generalized Bingham number (Bi). For high HB, large unyielded regions appear (Singh *et al.*, 2017); thus, this number describes the ratio between yield stress and viscous shear stress. The HB is given by Eq (1) (Chhabra and Richardson, 2011):

$$HB = \frac{\tau_0^H D^n}{m\bar{U}^n} \tag{1}$$

where τ_0^H is the yield stress, m the consistency coefficient, D the upstream pipe diameter and $\bar{U}$ is the mean velocity of the flow. Another important dimensionless parameter is the Hedström number for Herschel-Bulkley fluids (He_{HB}) (Malin, 1998), which correlates the rheological parameters of the fluid, and expresses a ratio between the yield stress and the consistency coefficient of the fluid; this number is given by Eq. (2):

$$He_{HB} = \frac{\rho D^2 \tau_0^{H(2/n-1)}}{m^{2/n}} \tag{2}$$

An interesting behavior of viscoplastic fluid flows is that the unyielded plug zone is reduced with high flow rates due to an increase of the viscous forces. Also, the velocity profile has a Newtonian fluid-like behavior when turbulent conditions are reached (Rudman *et al.*, 2004; Peixinho *et al.*, 2005; Chhabra and Richardson, 2011). Experimental studies have been performed to describe the behavior of viscoplastic fluids at different flow conditions using visualization techniques (Hammad *et al.*, 1999; Souza Mendes *et al.*, 2007), and measuring the energy losses through sudden contractions (Mika, 2011). These studies, in general, analyzed the influence of the Reynolds number and the steady-state rheological parameters on the flow behavior of viscoplastic fluids. Nevertheless, there are insufficient experimental data for reliable conclusions and comparisons with numerical and other experimental studies. Most of them are not focused on visualization of the flow behavior, and correlations with vortex structures formation and rheological parameters are hardly mentioned.

In the present work, an experimental study is conducted to visualize and analyze the flow structure before the contraction at different Reynolds and Hedström numbers. Also the effect of the contraction on the velocity profiles, generation of vortex structure, the variation of unyielded regions area and the behavior of pressure drop at the contraction, to fulfill the gap of the experimental data in the literature.

2. MATERIALS AND METHODS

2.1 Experimental Setup

The experimental setup used to carry out the present study consists of two systems. The first is a flow-loop presented in Fig 2.

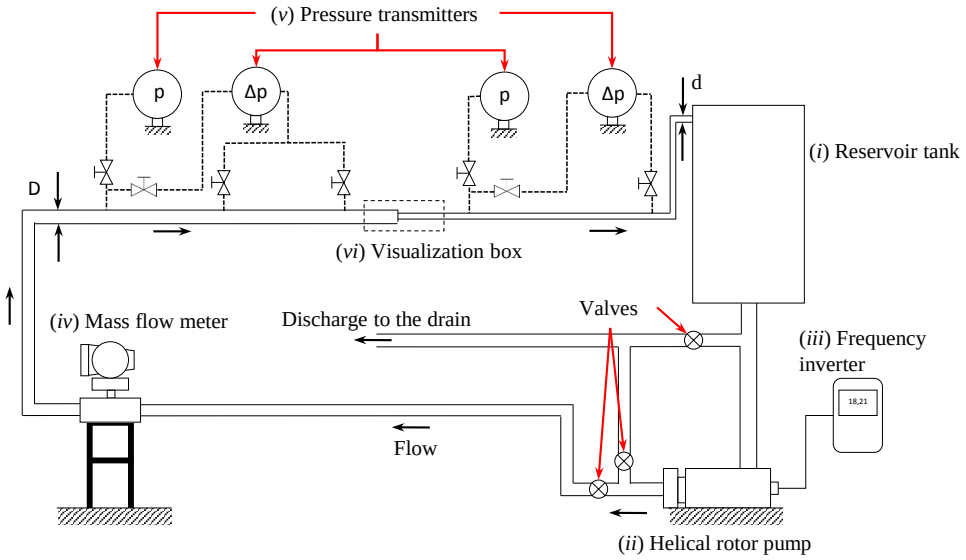

Figure 2. Experimental facilities: hydraulic system for tests performing.

The flow-loop facility is comprised of a 100 L tank (i) with a mixing system homogenizes the solution of ultrasound gel and water. The flow is provided by a helical rotor pump (NETZSCH mono pump) (ii) through a hydraulic circuit of

circular acrylic tubes and PVC (Polyvinyl chloride) pipes with 12.5 m of total length. The hydraulic system is an assembly of pipes with 25.9 mm of diameter (D) for the upstream zone, and 14 mm of the inside diameter (d) for the downstream zone of the contraction, obtaining a ratio contraction ($\beta = D/d$) of 1.85. The upstream zone before the contractions has 8.3 m length and allows a fully developed flow for laminar conditions. Flow rate is controlled by a frequency inverter (iii) with the aid of a mass flow meter (Micro-Motion) (iv). Temperature and density are measured as secondary outputs from the flow meter. For a given flow rate, the total error upon the mean velocity is estimated as 1 to 3%. Pressure transmitters (v) are used along the test section, before and after the visualization box (vi), to obtain differential pressure measurements. Pressure tappings of 4 mm internal diameter are connected to cylindrical tubings that are filled with de-ionized water and finally to the pressure transmitter (Rosemount). The accuracy of the transmitter is estimated at 0.1% for span range (0-62 mbar) and a total error of 0.4% for the full range of measurement (0-138 bar).

The second system is used for the visualization of the viscoplastic flow through the flow loop using a Particle Image Velocimetry (PIV) technique. The PIV is a non-intrusive technique that allows measuring local quantities information, and it is possible to evaluate the coupling between velocities at different points of the flow field and obtain the spatial distribution of the velocity Deshpande (2010). This technique uses a double-laser of 60 mJ, and a wavelength of 532 nm with a frequency of 100 Hz. The laser is synchronized with a CMOS camera to capture 1040 double frames images of the flow. Then, the images for frame 1 and frame 2 are processed and correlated with the assistance of Dantec Dynamics© software and Matlab™. Figure 3 shows the setup for using the PIV, and the images and the instantaneous vector field obtained by this technique. The laser system and the camera were set to 90 degrees in order to get a better visualization of the laser beam plane.

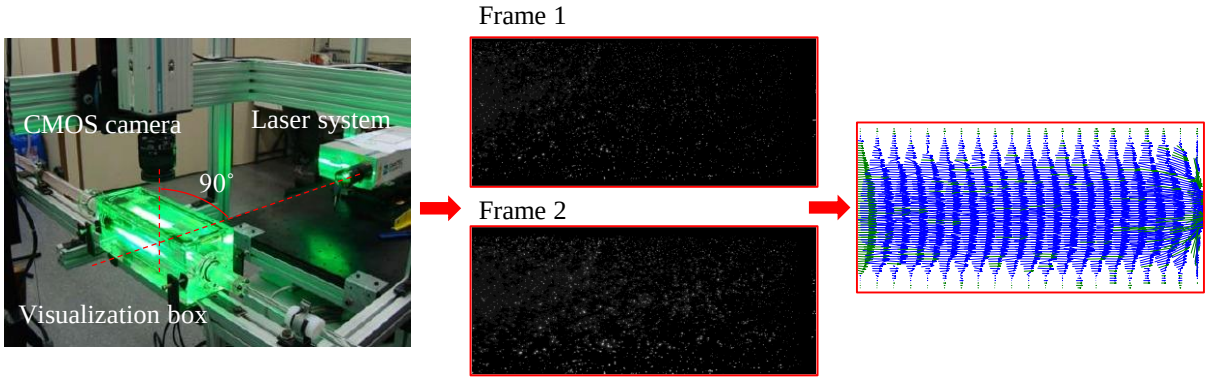

Figure 3. PIV setup for obtaining the double frame imaging and the instantaneous vector field correlation.

The Reynolds numbers were (Re'_D) set based on the Malin (1998) criterion to facilitate its control by the LabView platform and to compare the flow scalar maps. This is defined by the Eq. (3):

$$Re'_D = \frac{\rho \bar{U}^{2-n} D^n}{m(0.75 + 0.25/n)^n 8^{n-1}} \tag{3}$$

Nevertheless, in order to compare with some experimental studies in the literature, the values were led to Metzner and Reed (1955) correlation for a generalized Reynolds number ($Re_{D_{MR}}$) for non-Newtonian fluids. The $Re_{D_{MR}}$ is given by the expression:

$$Re_{D_{MR}} = \frac{\rho \bar{U}^{2-n'} D^{n'}}{m' 8^{n'-1}} \tag{4}$$

The parameters n' and m' depend on the rheological parameters obtained by the rheometer (Peixinho *et al.*, 2005). These are described by Eqs. (5) and (6) :

$$n' = \frac{(1-\phi) + 2\phi(1-\phi)(1+a)/(2+a) + (1-\phi)^2(1+a)/(3+a)}{a + 1 - 3(1-\phi)[\phi^2 + 2\phi(1-\phi)(1+a)/(2+a) + (1-\phi)^2(1+a)/(3+a)]} \tag{5}$$

$$m' = \left(\frac{m^a}{4}\right)^{n'} \left(\frac{\tau_0}{\phi}\right)^{1-n'a} \left\{(1-\phi)^{1+a}\left[1 + \frac{2(1-\phi)(1+a)}{\phi(2+a)} + \frac{(1-\phi)^2(1+a)}{\phi^2(3+a)}\right]\right\}^{-n'} \tag{6}$$

where $a = 1/n$ and ϕ are the ratio between the yield stress and the wall shear stress (τ_w/τ_0^H).

Table 1 summarized the Reynolds numbers set by the Malin (1998) and the equivalent generalized Reynolds number of Metzner and Reed (1955) at the entrance of the test section.

The generalized Reynolds numbers $Re_{D_{MR}}$ is used to correlate the first part of the results section of this paper, which are pressure losses and pressure loss coefficient at the contraction.

Table 1. Reynold numbers equivalence set at the present experimental study.

Fluid	**Reynolds number**							
40W	Re'_D	1	10	100				
	$Re_{D_{MR}}$	0.92	14	392				
30W	Re'	10	50	100	200	300	500	650
	$Re_{D_{MR}}$	15	113	339	1114	2332	3230	4167
20W	Re'_D	10	50	100	200	500	1000	1500
	$Re_{D_{MR}}$	75	941	4263	14113	124260	578462	1.87×10^6
10W	Re'_D	1500	2000	4000	5000	10000		
	$Re_{D_{MR}}$	2358	4949	41379	59470	617×10^6		

2.2 Rheological fluid characterization

In the choice of a properly viscoplastic fluid to be used in this study, some considerations were stated regarding viscosity, density, chemical compatibility, chemical stability, and physical properties. To achieve all aspects determined, Carbopol has been chosen. Such fluid was used in the study of Peixinho *et al.* (2005), that used an aqueous solution of 0.2% weight (wt) Carbopol 940 from B.F. Goodrich®, which was characterized as non-Newtonian fluid and fit by the Herschel-Bulkley model. Souza Mendes *et al.* (2007) used different aqueous solutions of Carbopol 676 that were characterized as viscoplastic fluid by the Herschel-Bulkley model. Stein (2005) studied 0.09%wt concentrations of Carbopol 676, which represent with a good agreement the viscoplastic behavior of drilling fluids. Then, for the current study, a commercial ultrasound gel is used with 40, 30, 20, and 10%wt diluted in water. This gel is composed of carboxyvinyl polymer (Carbopol 940), with a density of 950 kg/m^3, and it exhibits relevant viscoplastic fluid characteristics (Magnin and Piau, 1992; Piau, 2007). Figure 4 presents the steady flow curve and the viscosity curve behavior for the different ultrasound gel solutions. The rheological tests were performed in a HAAKE-MARS III (Modular Advanced Rheometer system) using cross-hatched parallel plates for shear rates below 50 s^{-1}, and concentric smooth cylinders configuration for shear rates between 50 and 1100 s^{-1}. The cross-hatched parallel plates with 35mm and 1 mm gap minimize the wall-slip effects in the rheometer for low shear rates (Fernandes *et al.*, 2019).

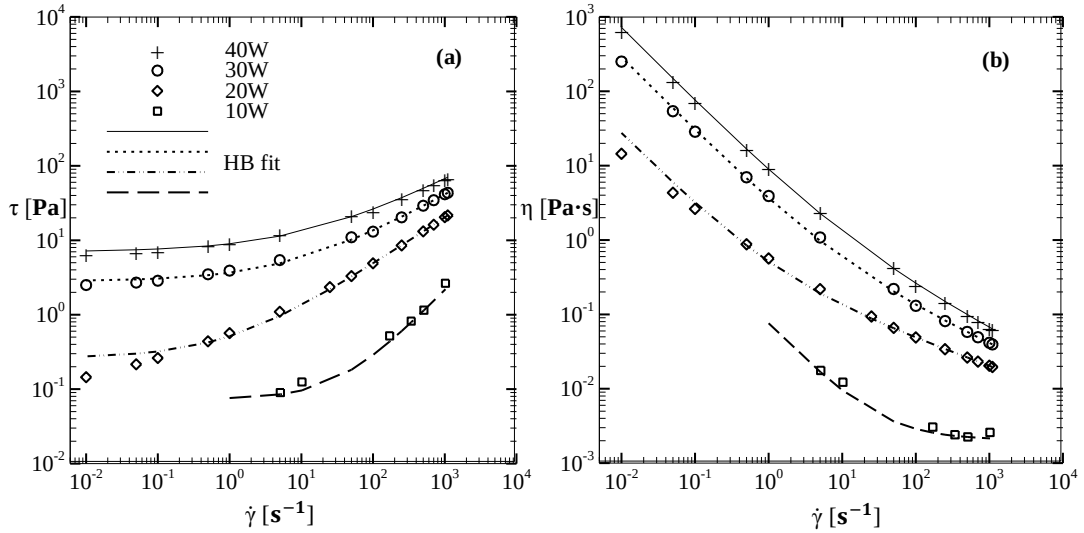

Figure 4. (a) Steady-state flow curve for the different ultrasound gel solutions well described by the Herschel-Bulkley model. (b) Viscosity behavior for the different solutions.

Table 2 shows the rheological parameters obtained after fitting the steady flow curves for each solution by the Herschel-Bulkley model. A high concentration of ultrasound gel means a higher τ_0^H and greater values for m; thus, the fluid is getting more viscous consistency. On the contrary, happens with n, a high concentration of ultrasound gel decreases the value for n, due to a higher consistency of the fluid means a reduction of the shear thinning behavior.

For 10W solution, there was not possible to calculate a He_{HB} value due to the low value for τ_0^H and $n \approx 1$ yields to a higher value than the other fluids. Nevertheless, based on the theoretical definitions of Malin (1998) for $n \approx 1$, He_{HB} reaches a value of 0, and its behavior can be fit as a Bingham fluid, a particular case for Herschel-Bulkley fluids.

Table 2. Herschel-Bulkley parameters and Hedström number calculated for ultrasound gel solutions.

Concentration	τ_0^H **[Pa]**	m **[Pa·s^n]**	n	He_{HB}
40%wt (40W)	6.994	1.976	0.495	16.402
30%wt (30W)	2.818	0.847	0.553	18.706
20%wt (20W)	0.262	0.251	0.634	2.938
10%wt (10W)	0.074	0.0023	0.986	-

3. METHODOLOGY VALIDATION

Calibration tests were carried out to validate the PIV technique with water as Newtonian fluid flow were performed for different Reynolds numbers. The data obtained were compared with Laser Doppler Velocimetry (LDV), and Direct Numeric Simulation (DNS) performed by Den Toonder and Nieuwstadt (1997) and Eggels *et al.* (1994), respectively. Axial velocity profile (u) and axial velocity fluctuations (u') were normalized by the friction wall velocity ($u^* = \bar{U}\sqrt{f/8}$) (Van Doorne and Westerweel, 2007). Then, the normalized velocities were obtained as: U^+=u/u^* and u'^+=u'/u^*, see Fig. 5 a)-d). An error of 1.1% is showed near to the pipe wall between DNS and experimental data, due to the refinement limitations of the PIV technique at the wall region.

The validation stage shows that the methodology used has a good agreement with the studies found in the literature for Newtonian and non-Newtonian fluid flows in straight pipes.

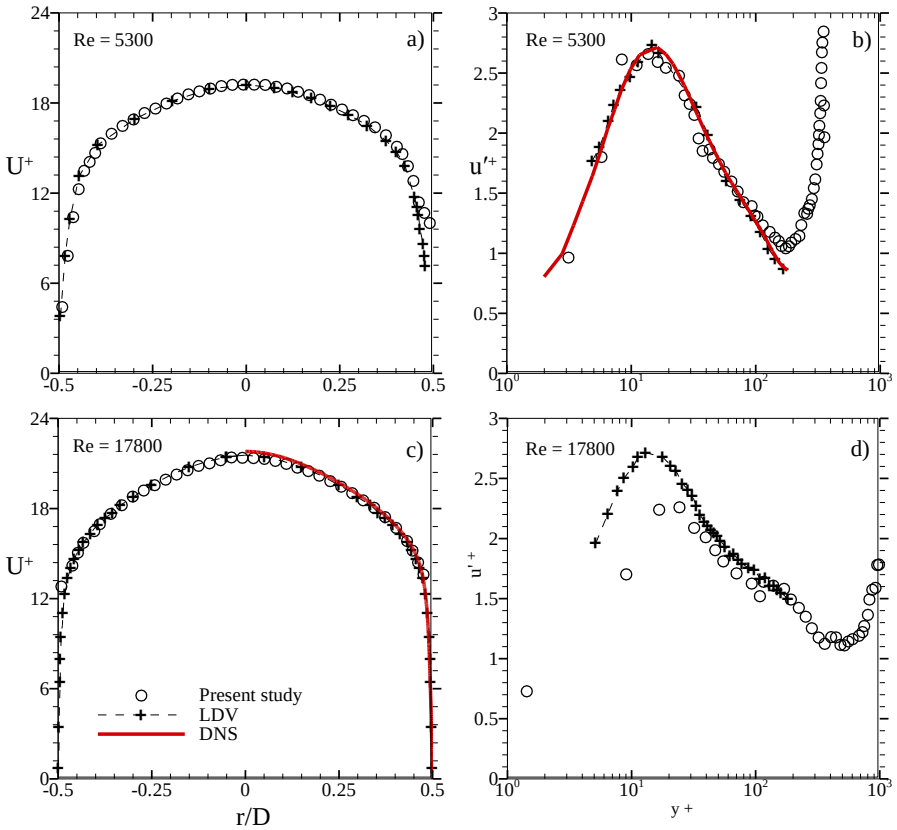

Figure 5. Normalized axial velocity profiles a), c) and and the axial velocity fluctuations b) and d) for water, obtained in the present study. Data were compared with LDV and DNS data at turbulent Reynolds numbers

4. RESULTS AND DISCUSSION

The results are presented in two parts. The first one is dedicated to the pressure drop behavior at the contraction and the pressure drop coefficient. The second part presents the behavior of the different viscoplastic fluids at different regimes.

4.1 Pressure losses

The pressure along the axial direction of the test section decreases linearly. This linear trend allowed to fit the pressure gradient using the least square method. The pressure gradients are shown in Fig. 6, upstream and downstream pressure gradients equations were extrapolated to the contraction plane ($Z/D = 0$), in order to calculate the pressure drop at the contraction (ΔP_{con}), using the equation $\Delta P_{con} = P_{c1} - P_{c2}$.

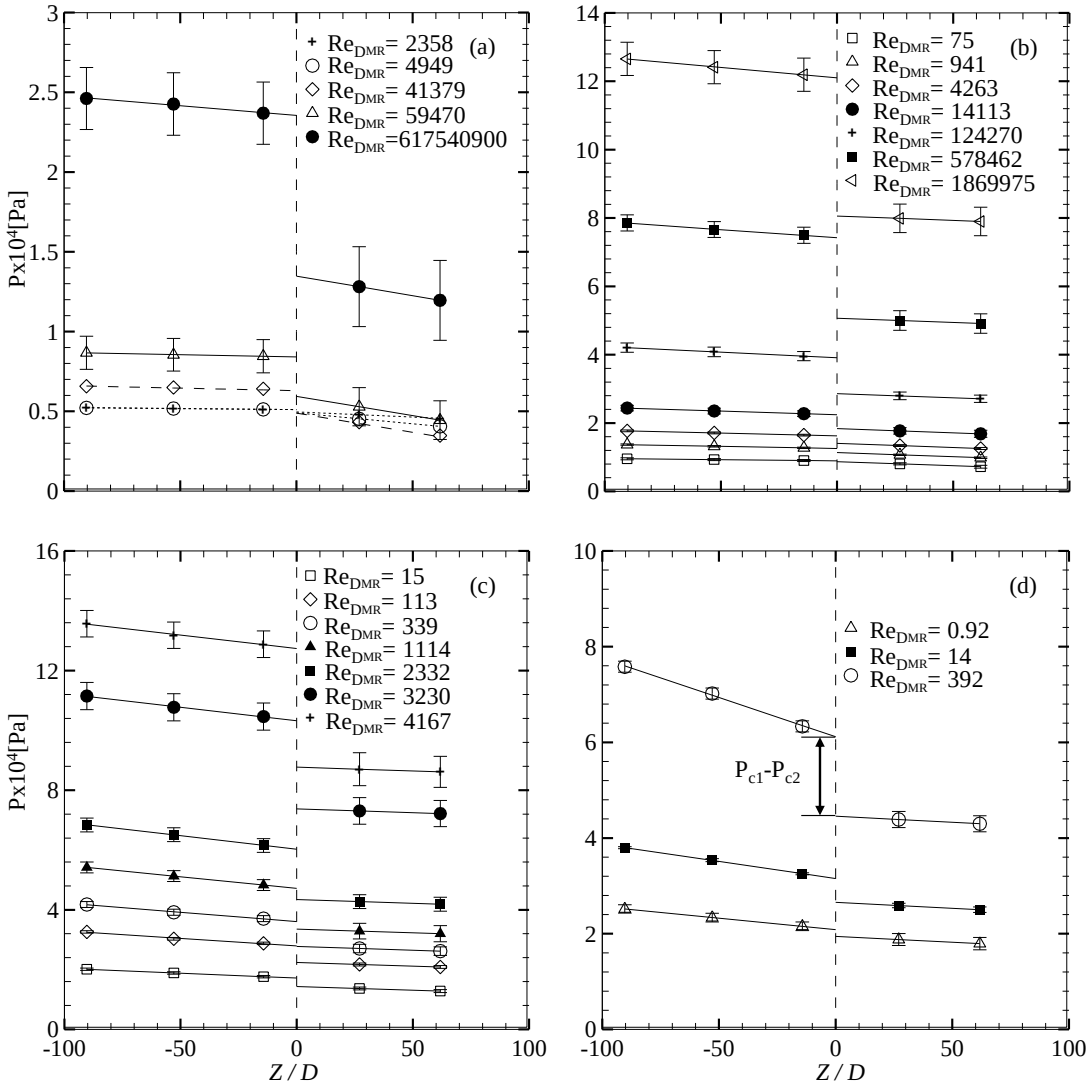

Figure 6. Pressure profiles along the flow-loop in function of the dimensionless distance from the contraction Z/D and the Reynolds number at the test section entrance, $Re_{D_{MR}}$. Each viscoplastic solution is presented: (a) 10W, (b) 20W, (c) 30W and (d) 40W.

The square value for the correlation coefficients (R^2) was calculated, obtaining a range between 1.000 and 0.991 and an average value of 0.999 for the upstream region of the contraction and 1.000 for the downstream one. Pressure values are presented in Pascal [Pa] trough the dimensionless axial distance from the contraction. The non-dimensionalization of the data was done with the test section entrance diameter (D).

From figure 6, it is possible to state that for high generalized Reynolds number at the entrance $Re_{D_{MR}}$, and high yield stress values, are required higher entrance pressures to keep the flow regime. The fluid 10W, with lower yield stress, presents low-pressure losses for $Re_{D_{MR}} < 5000$. This behavior is due to the low consistency and the high shear-thinning behavior of this fluid, hence, there is not necessary imposed high stress to keep the material flowing until high $Re_{D_{MR}}$ are reached and pressure losses are increased substantially at the downstream region.

For high $Re_{D_{MR}}$ values, the pressure drop at the contraction is increased. The increasing pressure drop is related to the increase of the Reynolds number values when the fluid passes through the contraction. As the velocity of the fluid is increased according to the continuity equations, the regime after the contraction varies concerning the Reynolds number at the entrance section according to the Metzner and Reed (1955) expression: $Re_{d_{MR}} = Re_{D_{MR}} \times \beta^{2(2-n')}$. Thus, the

value of n' is approximately 1 for the different viscoplastic solutions it is possible to state that $Re_{d_{MR}} \approx Re_{D_{MR}} \times \beta^2$, at the downstream region of the contraction a high Reynolds number is obtained, and the variations on the fluid behavior are more significant, and consequently the losses at the contraction are increased.

Also, at Figure 6 is depicted that the pressure drop at the contraction is increased as higher is the He_{HB}, for fluid 40W at $Re_{D_{MR}} = 392$ is found that $\Delta P_{con} = 16.6 \times 10^4$ Pa, and for fluid 30W $Re_{D_{MR}} = 339$ is $\Delta P_{con} = 8.3 \times 10^4$ Pa. This behavior is kind of contradictory with the stated by Nakamura and Sawada (1988), that for Bingham fluids, high He has an effect which decreases the pressure drop in the converging plane of a contraction. Nonetheless, for Herschel-Bulkley fluids, this behavior can vary according to the rheological parameters of these type of fluids. At the next subsection, the pressure loss coefficient at the contraction was obtained and compared with some experimental studies to validate the results obtained for the pressure drop.

4.2 Pressure loss coefficient

The pressure loss coefficient is calculated with the equation used in experimental studies by Fester *et al.* (2008) :

$$k_{con} = \frac{(\Delta p_{con}/\rho g) + (\alpha_1 \bar{U}_1^2 - \alpha_2 \bar{U}_2^2)/2g}{\bar{U}_2^2/2g} \tag{7}$$

where α_1, α_2, $\bar{U}_1$ and $\bar{U}_2$ are the kinetic energy correction factor and the mean velocity at the downstream and upstream region of the contraction. The values for α_1 and α_2 were calculated with the correlations presented by Mika (2011). These correlations are based on the Strzelecka and Jezowiecka-Kabsch (2008) criteria, used for non-Newtonian fluid flows at turbulent regime. Equation 8 related the kinetic energy correction factor with the generalized Reynolds number.

$$\alpha = 1 + 105\left(\frac{10}{\ln^2 Re_{MR}}\right)^3 - 11.88\left(\frac{10}{\ln^2 Re_{MR}}\right)^2 + 1.208\left(\frac{11.3}{\ln^2 Re_{MR}}\right) \tag{8}$$

For laminar flow conditions the correlation calculated by Mika (2011) is based on the shear stress ratio ϕ:

$$\alpha = \frac{54\left(47\phi^2 + 58\phi + 35\right)}{35\left(\phi^2 + 2\phi + 3\right)^3} \tag{9}$$

Figure 7 shows the behavior of the loss pressure coefficient calculated for each concentration at the different Reynolds numbers. For a log-log plot, the laminar Reynolds depicts a linear behavior. Instead, for Reynolds greater than 3000, K_{con} reaches a constant value. In the literature, there are mainly two models to fit the pressure loss coefficient. One of these methods is K's method presented by Hooper (1981) and expressed by:

$$K = \frac{k_1}{Re} + k_\infty \tag{10}$$

where k_1 is the coefficient related to a decreasing behavior at the laminar regime. So k_∞ is the constant behavior reaches the turbulent regime.

For the present study, the fit K's values were set as k_1=783.19 and k_∞=2.668, given the follow representative equation for the pressure loss coefficient at the contraction:

$$K_{con} = \frac{783.19}{Re_{D_{MR}}} + 2.668 \tag{11}$$

The correlation is compared with some found in the literature, as Turian *et al.* (1998); Fester *et al.* (2008) and Mika (2011). The firsts stated correlations with rational functions, $900/Re_{D_{MR}}$ and $288/Re_{D_{MR}}$, respectively. Mika (2011) fit the experimental values by a power function given by $11000/Re_{D_{MR}}^{1.26}$. On the other hand, for the turbulent Reynolds numbers each correlation reach different constant values, 1.114 by Turian *et al.* (1998) and 0.38 by Mika (2011). However, in these studies it is highlighted that the correlation for loss pressure coefficients is sensible to geometrical and rheological parameters; for that reason, it is not possible to lead to a global correlation for viscoplastic fluids.

Nonetheless, the behavior for the different fluid shows a critical Reynolds number, hence, for $Re_{D_{MR}}$ >2000, where the K_{con} values reach an asymptotic value (k_∞), it seems to be constant in any event for each viscoplastic solution, but it is important to note that this value can be different for each experimental design and the particular type of piping elements through the flow-loop.

4.3 Flow field and mean quantities

The mean velocity vector map was obtained using the PIV technique and the assistance of software to correlate the images obtained. Through the correlation of the displacement of seeding particles was calculated a vector for each position

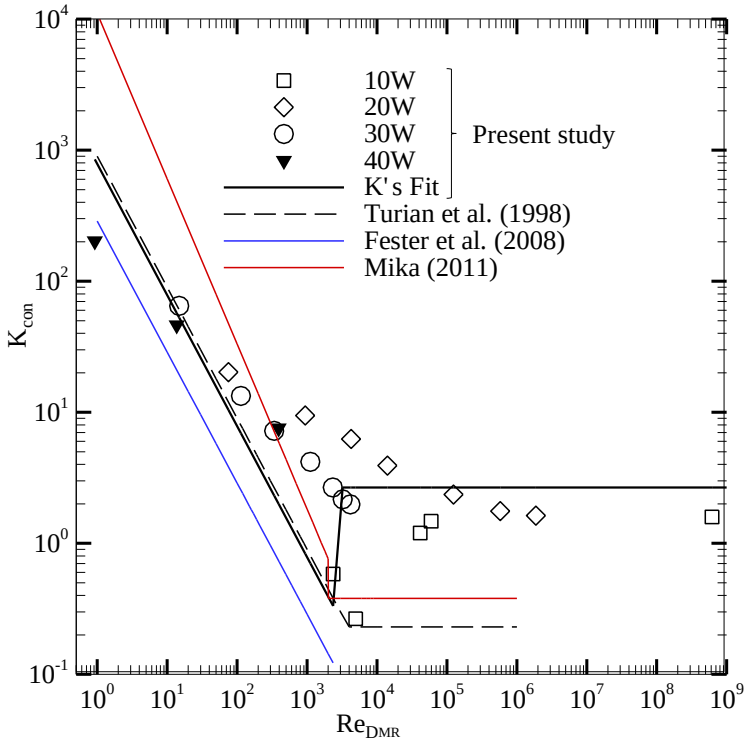

Figure 7. Pressure loss coefficient at the contraction in function of the Reynolds number at the entrance section. Experimental values fit by K's method proposed by Hooper (1981) and compare with other viscoplastic fluid flow correlations.

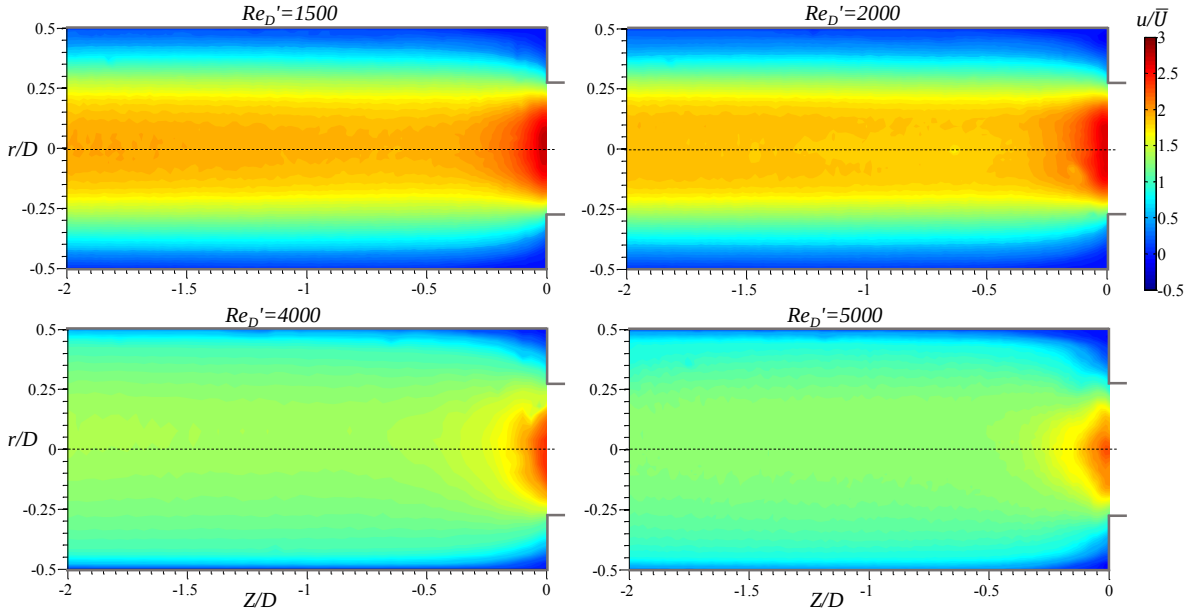

Figure 8. Dimensionless axial velocity component $u/\bar{U}$ for different Re'_D set for viscoplastic fluid 10W.

of the test section, and then a statistic from multiple vector maps was done to obtain a single vector map. From this vector map were calculated the mean axial and radial velocities, as well as the shear rate and vorticity maps.

Figure 8 illustrates the axial velocity mean flow for a solution 10W. When the Re'_D increases, the dimensionless velocity $u/\bar{U}$ decreases along the upstream region, including the region near to the contraction. Hence, as the turbulent regime is reached the velocity profile presents a flat shape.

Figure 9 shows the evolution of the velocity profile through the test section before the contraction plane. Near to the contraction, the axial and radial velocity gradients increase drastically, and thus, the shear rate increases. The high shear rates reduced the plug region (dot-dashed line), near to Z=-0.1D the plug has almost disappeared and the velocity increase at the entrance of the contraction as a function of β, as it was referenced at the validation section, and reaching values of

2.5 for the dimensionless velocity $u/\bar{U}$.

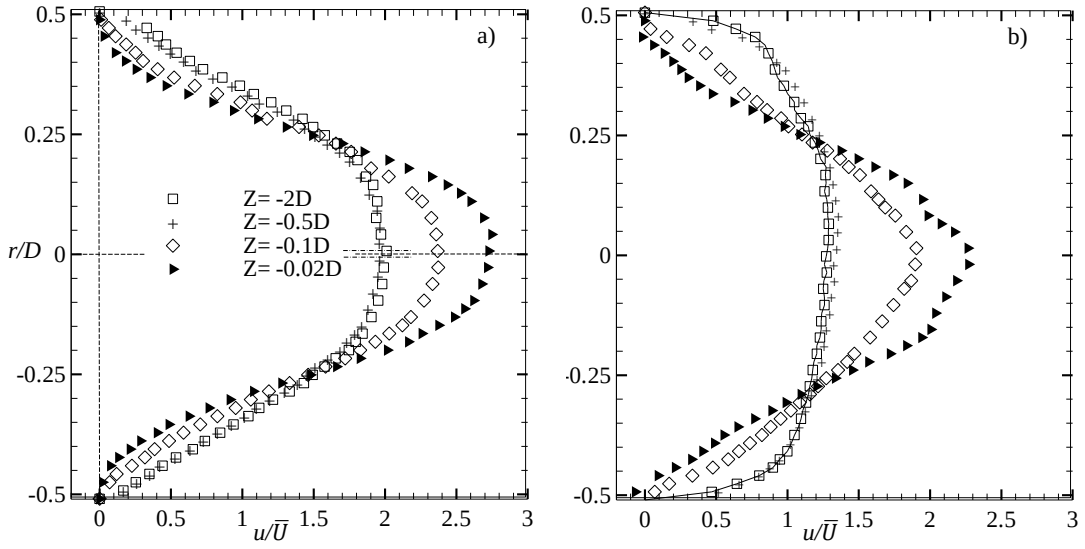

Figure 9. Dimensionless axial velocity component $u/\bar{U}$ for fluid 10W in different Re'_D: a) 1500, b)5000. Dash-dotted lines represent the plug core diameter.

Figure 9(b) show for turbulent Re'_D at the entrance of the test section (Z= $-2D$), flat shape is presented, and the core plug has vanished, and $u/\bar{U}$ has a uniform distribution along the section visualized. At position Z=$-0.02D$ the velocity profile presents a reverse flow near to the wall for turbulent Re'_D. This secondary flow is generated by the vortex structures formed at the corner of the contraction, that increases his intensity as the Re'_D is increased. At the following subsections, this topic is discussed.

4.4 Plug core structure

The plug core size increases with the yield stress, as higher values for τ_0^H and HB, more unyielded areas are presented in the flow structure. For viscoplastic solution, the ratio $u/\bar{U}$ decreases for low n and high τ_0^H, which means that for high HB and He_{HB} values the fluid presents a greater plug core structure, this is depicted in Fig. 10, where is shown a comparison of the velocity profiles at $Z = -2D$ for each solution and different Reynolds number, Re'_D.

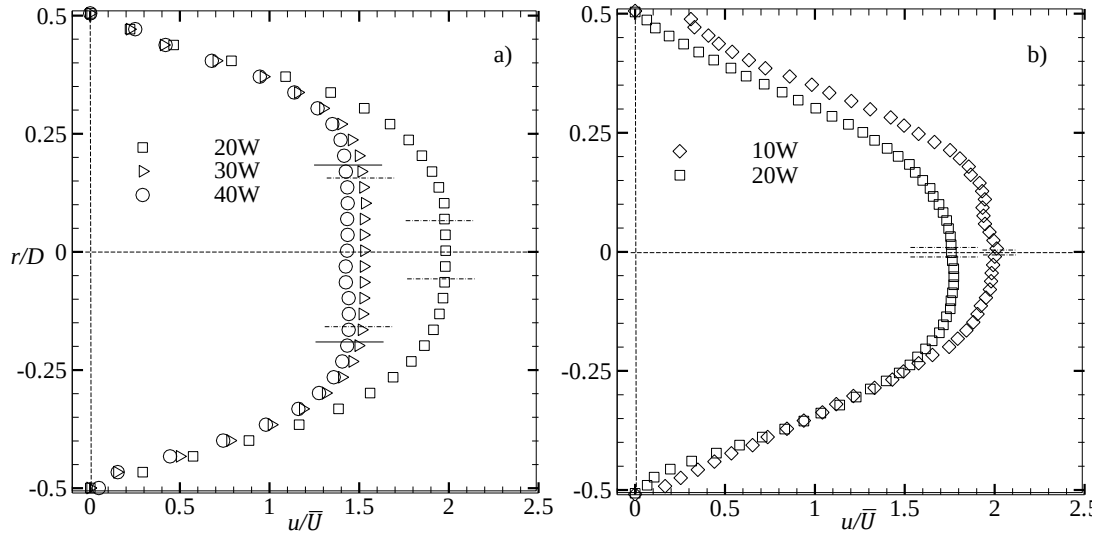

Figure 10. Comparison of the velocity profile and the plug core size at Z=$-2D$ for different Re'_D: a) 10, b) 1500.

For the laminar Reynolds numbers, Re'_D=10 and 100, the ratio $u/\bar{U}$ reaches a value of 1.5 for fluid 30W and 40W. Instead of the fluid 20W that has a lower yield stress value, this ratio reaches values between 1.8 and 2. The plug core radius r_p for Re'_D=10 varies for each solution at the entrance of the test section for fluid 40W is $0.187D$, instead of fluid 30W is $0.173D$ and for 20W is $0.067D$. These values represent 38%, 35%, and 13% of the entrance area. When the Re'_D is increased to 100, the value for rp is reduced to $0.149D$, $0.103D$ and $0.032D$ for 40W, 30W and 20W, respectively.

As the Reynolds number reaches transitional values, $u/\bar{U}$ trends to 2, the $u/\bar{U}$ ratio reached by Newtonian fluids in laminar flows. For values of n near to 1, this ratio is achieved, and there is a presence of a tiny plug core region, for a $Re'_D = 1500$ the value for rp is reduced to $0.009D$ for fluid 20W and $0.001D$ for 10W.

The rheological properties affect the reduction of the plug core area directly when the Reynolds number increases. High τ_0^H and low n values generate larger plug regions and maintain the unyielded region including at transitional Re'_D. Instead, low τ_0^H and high n lead to a sudden deformation of the plug core and like Newtonian behavior for viscoplastic fluids, that means for each viscoplastic fluid there is a critical Re'_D where the unyielded regions disappear, and the fluid reaches a behavior like a Newtonian fluid. This behavior agrees with the correlations Hanks *et al.* (1967), Hanks (1963), and Malin (1998), which stated that exist a critical Reynolds number Re_c where the yield-stress fluids change their behavior, but this value varies as a function of the He. For Hedström numbers below 1000, the critical Reynolds number is set between 2000 and 2100, (Hanks *et al.*, 1967).

Figure 10 d) shows that the velocity for 20W and 10W present an asymmetry profiles for a $Re'_D = 1500$. As stated by Escudier and Presti (1996) and Peixinho *et al.* (2005) the viscoplastic fluids has this particular behavior for Re'_D at the transitional regime, more specific when Re'_D reaches the critical value. According to the Malin (1998) correlation, fluids 10W and 20W have a critical Reynolds number of 2000 and 2100, respectively. As it was mentioned in the validation section, this asymmetry profile is presented due to an instability of the flow presented for transitional regimes, where are generated turbulent spots. This behavior is a topic of ongoing researches.

4.5 Vortex structures

Vortex structures are possible to identify analysing the velocity gradient tensor $\bigtriangledown\mathbf{u}$. The most widely used schemes to identify vortex are the Q criterion of Hunt *et al.* (1988), the Lambda-2 criterion of Hussain and Jeong (1995) and the Δ criterion proposed by Chong *et al.* (1990). The analysis of $\bigtriangledown\mathbf{u}$ provides a rational basis for vortex identification, using the velocity gradient decomposition:

$$\bigtriangledown\mathbf{u} = \mathbf{S} + \mathbf{\Omega} \tag{12}$$

where $\mathbf{S} = 1/2((\bigtriangledown\mathbf{u}) + (\bigtriangledown\mathbf{u})^t)$ is the symmetric (rate of strain tensor) and $\mathbf{\Omega} = 1/2((\bigtriangledown\mathbf{u}) - (\bigtriangledown\mathbf{u})^t)$ the antisymmetric component (rate of rotation tensor) of $\bigtriangledown\mathbf{u}$. Considering $\mathbf{S^2} + \mathbf{\Omega^2}$, the eigenvalues for this symmetric tensor are real. If λ_1, λ_2 and λ_3 are the eigenvalues and $\lambda_1 \geq \lambda_2 \geq \lambda_3$, at least two of these eigenvalues will be negative when the point under analysis is part of a vortex, corresponding to the Lambda-2 vortex criterion requiring simply $\lambda_2 < 0$.That means that the vorticity magnitude (solid-body rotation) prevails over the strain rate magnitude (deformation).

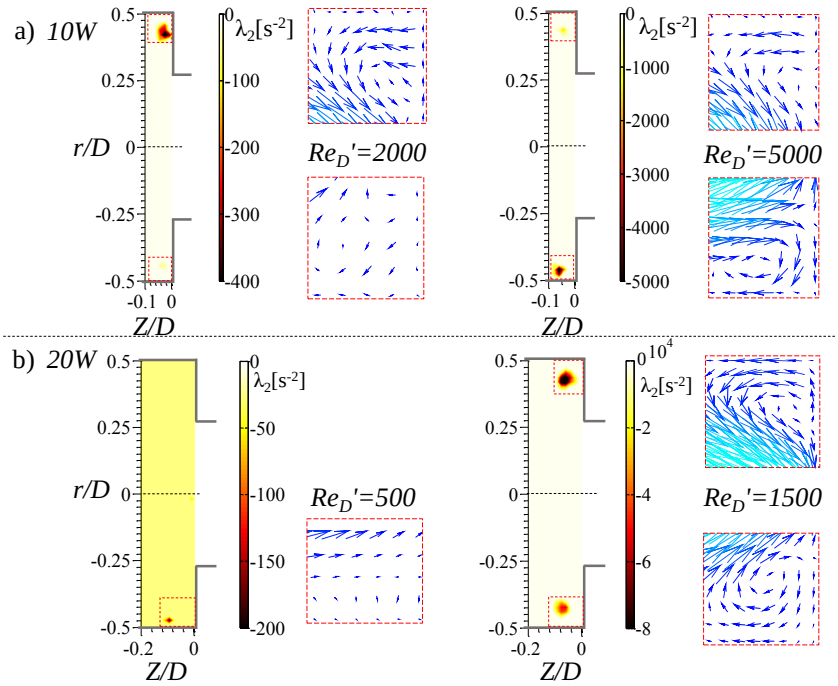

Figure 11. Vortex structure detection with lambda criteria at different Reynolds numbers: a) for fluid 10W, and b) for fluid 20W.

Figure 11 shows the analysis led for 10W and 20W solutions using the Lambda-2 criterion. The values obtained allow to identify the area where there is a prevalence of vorticity; high values mean high vorticity rates. The limits of the area

under the effect of solid-body rotation are considered when the values obtained for λ_2 reach 0. For the 10W fluid at Re'_D=1500, the vortex structure starts its formation with low vorticity rates and near to the corner walls, at Z/D=-0.04. When Re'_D is increased, the size of the area affects by the vorticity, represents by a square, starts to increase at the laminar regime. After turbulent Re'_D are reached, the size of the area starts to decrease but presents higher vorticity rates, that means a concentration of the solid-body rotation effect, constant viscosity areas. For Re'_D=2000, the sides of the area are $\approx 0.1D$, whereas for Re'_D=5000 these decrease to $\approx 0.06D$. It is possible to state that the vortex starts to move backward when the turbulent regime is reached, for Re'_D=5000 the area under the effect of vorticity is located atZ/D=-0.06.

On the other hand, for 20W fluid, the formation of the vortex structure starts with a Re_D=500. As this value is increased, higher rates of vorticity are generated, and the sides of the area affected increases from $\approx 0.04D$ to $\approx 0.08D$. In contrast with 10W, the formation of the vortex structures for 20W fluid starts at Z/D=-0.1, farther than the vortex structures for 10W. The fluid near the corners of the contraction has low velocities due to the presence of yield stress. As the yields stress increases the velocity of this section is lower, making a barrier for the formation of the vortex structures that are generated farther from the corner walls. As the $Re'D$ is increased, the vortex starts to move forward, due to the deformation of these regions have increased, modifying the velocity field at the corners of the contraction. It is possible to appreciate this behavior with the vectorial maps at the corner regions present in Figure 11. The vector maps at the corners of the contraction show low values for the velocity magnitude at laminar $Re'D$.

5. CONCLUSIONS

The study and the visualization of the viscoplastic fluid flow through axisymmetric contraction allowed to establish correlations of the flow structure and the rheological properties: High He_{HB} means large plug cores and unyielded regions, reducing the effective flow area. Also, high τ_0^H values difficult the flow of the fluid, and high entrance pressures are required to lead the flow at turbulent regimes. For Re'_D near to the transitional regime, an asymmetric behavior is presented. This condition is associated with the generation of turbulent spots and the sensibility of the flow with geometrical changes along the flow-loop. As turbulent Reynolds numbers are reached, the viscoplastic fluids present a shear-thinning behavior reducing the unyielded regions, and promoting the generation of secondary flows as vortex structures. As the Re'_D is increased at the turbulent regime, the area affects by the vortex structures is reduced, and the unyielded regions are vanished due to the high shear rates generated by the pressure drop at the contraction plane. Nevertheless, such behavior is easily reached by viscoplastic fluids with low τ_0^H values and $He_{HB} < 10$, allowing larger effective flow areas and low-pressure losses.

6. ACKNOWLEDGMENTS

This work has been supported by the Federal University of Technology-Parana's Research Center for Rheology and Non-Newtonian Fluids-CERNN.

7. REFERENCES

Chhabra, R.P. and Richardson, J.F., 2011. *Non-Newtonian flow and applied rheology: engineering applications*. Butterworth-Heinemann.

Chong, M.S., Perry, A.E. and Cantwell, B.J., 1990. "A general classification of three-dimensional flow fields". *Physics of Fluids A: Fluid Dynamics*, Vol. 2, No. 5, pp. 765–777.

Den Toonder, J. and Nieuwstadt, F., 1997. "Reynolds number effects in a turbulent pipe flow for low to moderate re". *Physics of Fluids*, Vol. 9, No. 11, pp. 3398–3409.

Deshpande, A.P., 2010. "Piv techniques in experimental measurement of two phase (gas-liquid) systems". In *Rheology of complex fluids*, Springer, pp. 111–129.

Eggels, J., Unger, F., Weiss, M., Westerweel, J., Adrian, R., Friedrich, R. and Nieuwstadt, F., 1994. "Fully developed turbulent pipe flow: a comparison between direct numerical simulation and experiment". *Journal of Fluid Mechanics*, Vol. 268, pp. 175–210.

Escudier, M. and Presti, F., 1996. "Pipe flow of a thixotropic liquid". *Journal of Non-Newtonian Fluid Mechanics*, Vol. 62, No. 2-3, pp. 291–306.

Fernandes, R.R., Turezo, G., Andrade, D.E., Franco, A.T. and Negrão, C.O.R., 2019. "Are the rheological properties of water-based and synthetic drilling fluids obtained by the fann 35a viscometer reliable?" *Journal of Petroleum Science and Engineering*, Vol. 177, pp. 872–879.

Fester, V., Mbiya, B. and Slatter, P., 2008. "Energy losses of non-newtonian fluids in sudden pipe contractions". *Chemical Engineering Journal*, Vol. 145, No. 1, pp. 57–63.

Hammad, K.J., Otugen, M.V., Vradis, G.C. and Arik, E.B., 1999. "Laminar flow of a nonlinear viscoplastic fluid through an axisymmetric sudden expansion". *Journal of fluids engineering*, Vol. 121, No. 2, pp. 488–495.

Hanks, R.W., 1963. "The laminar-turbulent transition for fluids with a yield stress". *AIChE Journal*, Vol. 9, No. 3, pp.

306–309.

Hanks, R.W. *et al.*, 1967. "On the flow of bingham plastic slurries in pipes and between parallel plates". *Society of Petroleum Engineers Journal*, Vol. 7, No. 04, pp. 342–346.

Hooper, W.B., 1981. "The 2-k method predicts head losses in pipe fittings". *Chemical Engineering*, Vol. 88, No. 17, pp. 96–100.

Hunt, J.C., Wray, A.A. and Moin, P., 1988. "Eddies, streams, and convergence zones in turbulent flows".

Hussain, F. and Jeong, J., 1995. "On the identification of a vortex". *J. Fluid Mech*, Vol. 285, pp. 69–94.

Jay, P., Magnin, A. and Piau, J.M., 2002. "Numerical simulation of viscoplastic fluid flows through an axisymmetric contraction". *Journal of fluids engineering*, Vol. 124, No. 3, pp. 700–705.

Kfuri, S.L., Silva, J.Q., Soares, E.J. and Thompson, R.L., 2011. "Friction losses for power-law and viscoplastic materials in an entrance of a tube and an abrupt contraction". *Journal of Petroleum Science and Engineering*, Vol. 76, No. 3-4, pp. 224–235.

Kim-e, M., Brown, R. and Armstrong, R., 1983. "The roles of inertia and shear-thinning in flow of an inelastic liquid through an axisymmetric sudden contraction". *Journal of non-Newtonian fluid mechanics*, Vol. 13, No. 3, pp. 341–363.

Magnin, A. and Piau, J., 1992. "Flow of yield stress fluids through a sudden change of section". In *Theoretical and Applied Rheology*, Elsevier, pp. 195–197.

Malin, M., 1998. "Turbulent pipe flow of herschel-bulkley fluids". *International communications in heat and mass transfer*, Vol. 25, No. 3, pp. 321–330.

Metzner, A. and Reed, J., 1955. "Flow of non-newtonian fluidsâĂŤcorrelation of the laminar, transition, and turbulent-flow regions". *Aiche journal*, Vol. 1, No. 4, pp. 434–440.

Mika, L., 2011. "Energy losses of ice slurry in pipe sudden contractions". *Experimental Thermal and Fluid Science*, Vol. 35, No. 6, pp. 939–947.

Nakamura, M. and Sawada, T., 1988. "Numerical study on the flow of a non-newtonian fluid through an axisymmetric stenosis". *Journal of Biomechanical Engineering*, Vol. 110, No. 2, pp. 137–143.

Peixinho, J., Nouar, C., Desaubry, C. and Théron, B., 2005. "Laminar transitional and turbulent flow of yield stress fluid in a pipe". *Journal of Non-Newtonian Fluid Mechanics*, Vol. 128, No. 2-3, pp. 172–184.

Piau, J., 2007. "Carbopol gels: Elastoviscoplastic and slippery glasses made of individual swollen sponges: Meso-and macroscopic properties, constitutive equations and scaling laws". *Journal of non-newtonian fluid mechanics*, Vol. 144, No. 1, pp. 1–29.

Rudman, M., Blackburn, H.M., Graham, L. and Pullum, L., 2004. "Turbulent pipe flow of shear-thinning fluids". *Journal of non-newtonian fluid mechanics*, Vol. 118, No. 1, pp. 33–48.

Singh, J., Rudman, M. and Blackburn, H., 2017. "The effect of yield stress on pipe flow turbulence for generalised newtonian fluids". *Journal of Non-Newtonian Fluid Mechanics*, Vol. 249, pp. 53–62.

Souza Mendes, P.R., Naccache, M.F., Varges, P.R. and Marchesini, F.H., 2007. "Flow of viscoplastic liquids through axisymmetric expansions–contractions". *Journal of Non-Newtonian Fluid Mechanics*, Vol. 142, No. 1-3, pp. 207–217.

Stein, E., 2005. "Displacement of non-newtonian liquids in eccentric annuli". *Master Thesis, Rio de Janeiro, Brasil, Pontifícia Universidade Católica do Rio de Janeiro - PUC-RIO*.

Strzelecka, K. and Jezowiecka-Kabsch, K., 2008. "Coriolis coefficient in transitional and turbulent pipe flow". *OCHRONA SRODOWISKA*, Vol. 30, No. 1, pp. 21–25.

Turian, R., Ma, T.W., Hsu, F.L., Sung, M.J. and Plackmann, G., 1998. "Flow of concentrated non-newtonian slurries: 2. friction losses in bends, fittings, valves and venturi meters". *International journal of multiphase flow*, Vol. 24, No. 2, pp. 243–269.

Van Doorne, C. and Westerweel, J., 2007. "Measurement of laminar, transitional and turbulent pipe flow using stereoscopic-piv". *Experiments in Fluids*, Vol. 42, No. 2, pp. 259–279.

8. RESPONSIBILITY NOTICE

The authors are the only responsible for the printed material included in this paper.